CrystEngComm

ROYAL SOCIETY OF CHEMISTRY

PAPER

View Article Online
View Journal | View Issue

Cite this: *CrystEngComm*, 2022, **24**, 6642

Interfacial modulation and plasmonic effect mediated high-brightness green light sources in a single Ga-doped ZnO microwire based heterojunction

Xingjie Liu,[a] Maosheng Liu,[a] Rongde Zhu,[a] Binghui Li,*[b] Peng Wan,[a] Daning Shi,[a] Caixia Kan [a] and Mingming Jiang *[a]

Received 5th July 2022,
Accepted 29th August 2022

DOI: 10.1039/d2ce00917j

rsc.li/crystengcomm

Heterostructure manufacturing has been extensively studied as an indispensable footstone in progressive semiconductor optoelectronic devices due to the constituent materials, interfacial states and electronic transport capabilities, thus enabling competitive candidates to construct novel devices and expand new academic fields. Herein, we proposed and constructed a unique green light-emitting diode (LED), which contains a Ga-doped ZnO microwire covered with Au nanoparticles (AuNPs@ZnO:Ga MW), a MgO buffer layer and a p-type InGaN template. The LED can exhibit high-brightness, highly-stable and nearly droop-free green light-emitting features. To probe into the electroluminescence mechanism, a band alignment modification at the ZnO:Ga/InGaN heterointerface can be fulfilled in the presence of a MgO buffer layer, which can effectively avoid the electron–hole recombination occurring at the InGaN side. Meanwhile capping AuNPs can availably achieve strengthening of the charge transport properties, enhancement of the forward current density of the diode, and magnification of the green light emission on the basis of the plasmonic effect. The carefully designed LED structures revealed much superior electroluminescence properties over a broad scope of carrier density because of the improvement of hole injection and electron confinement, thus moderately suppressing the efficiency droop induced by InGaN materials. This work provides clear grounds for the achievement of high-efficiency visible light sources and understanding the microscopic mechanism of reducing the electron leakage, increasing the hole injection efficiency and enhancing the electroluminescence efficiency.

1 Introduction

The development of low-cost, high efficiency, wavelength-tunable semiconductor light emitting diodes (LEDs) has the potential to dramatically decrease global electricity consumption and greenhouse gas production. Currently, InGaN/GaN multi-quantum-well materials and structures have been intensively studied and identified as an emerging platform for constructing wavelength-tunable LEDs due to their continuously variable bandgap ranging from 0.7 to 3.4 eV.[1–6] Particularly, display technology based on micro- and nano-sized LEDs has attracted significant attention for comprehensive applications, including ultrahigh resolution lighting and displays, biomedical imaging, augmented/virtual reality, sensing, *etc.* For nearly two decades, painstaking efforts have been carried out to shrink the areal sizes of traditional InGaN-based materials, structures and devices.[7–10] Various attempts have been made to construct micro- and nanosized InGaN-based LEDs, which are mainly divided into two major categories: InGaN materials and low-dimensional structures can be prepared in heteroepitaxy (1) involving bottom-up growth methods[10–13] and (2) an alternative top-down experimental scheme, consisting of nanoimprint lithography, dry etching and wet chemical etching techniques.[14–18] Using bottom-up growth methods, low-dimensional GaN(InGaN) structures have been prepared using various kinds of experimental approaches, such as metal–organic chemical vapor deposition, catalyst-assisted vapor transport deposition, self-assembly methods, *etc.* Nevertheless, all these bottom-up preparation approaches require precise operation of the complicated growth conditions and complicated and expensive epitaxial growth equipment, and the fabrication procedure is time-consuming. Meanwhile,

[a] *College of Physics, MIIT Key Laboratory of Aerospace Information Materials and Physics, Key Laboratory for Intelligent Nano Materials and Devices, Nanjing University of Aeronautics and Astronautics, No. 29 Jiangjun Road, Nanjing 211106, China. E-mail: mmjiang@nuaa.edu.cn*
[b] *State Key Laboratory of Luminescence and Applications, Changchun Institute of Optics Fine Mechanics and Physics, Chinese Academy of Sciences, Changchun 130033, China. E-mail: binghuili@163.com*

these methods also brought about growth defects such as stacking faults or inversion domain boundaries.[8,19–21] By comparison, the preparation of high quality low-dimensional InGaN(GaN) structures using etching techniques still faces significant challenges, such as well-controlled features with vertical sidewalls and high-aspect-ratio structures due to the slight lateral etching.[15,22–24] Despite the comprehensive implementation of low-dimensional InGaN(GaN) display technology, many characteristics of these materials, structures and devices remain highly contentious, in particular the fountainhead of the efficiency droop phenomenon, which is caused by various nonradiative carrier loss mechanisms during the carrier transport process and carrier recombination process.[25–28]

As discussed previously, developing heterostructures is of critical significance for various optoelectronic devices, such as photodetectors, field-effect/bipolar transistors, LEDs, laser diodes, *etc.* In general, heterostructures have comparatively better electrical and optical performances with respect to their layered materials. The charge transport mechanism highly depends on various parameters including semiconductor materials, energy band alignments, interfacial characteristics, electronic transport features, and so on.[29–31] For the past decades, a combination of p-type InGaN materials and other n-type semiconductors with appropriate electronic band structures, carrier charge injection and transport paths, and controlled electron–hole recombination regions in carefully constructed heterostructures is significance for scientific research and realistic applications.[32,33] Due to its direct broad-bandgap of ~3.37 eV and high exciton binding energy of ~60 meV, ZnO has been generally believed as one of the most superior electroluminescent and laser gain materials. Thus, ZnO is most likely the critical compound for creating droop-free light-emission devices.[34–36] Particularly, various kinds of ZnO micro/nanostructures having controlled sizes and different morphologies have been successfully prepared, such as zero-dimensional quantum dots and nanocrystals,[37–40] one-dimensional wire-type structures (including nanowires, nanorods, nanoribbons and so on),[41–43] two-dimensional structures (such as nanoplates, nanosheets and nanodisks),[44–46] and three-dimensional flower-like and urchin-like hierarchical structures.[47,48] Through the appropriately designed n-ZnO/p-InGaN heterointerface, the combination of the merits of both the mature p-InGaN material and ZnO nano-/microstructures would make the as-designed low-dimensional visible light source technically and practically competitive.[33,49,50]

In the present research, a new generation high-brightness green LED, which is made of a single Ga-doped ZnO microwire covered with Au nanoparticles (AuNPs@ZnO:Ga MW), a MgO buffer layer and a p-type InGaN film, was proposed and investigated experimentally. The LED showed stable green electroluminescence (EL) peaking at around 545 nm, with a spectral line-width of ~40 nm. To probe into the EL mechanism, inserting a MgO buffer layer between the n-ZnO:Ga MW and p-InGaN heterointerface can be used to modulate the transport path of the injected carrier charges, thus achieving electron–hole recombination toward the band offset in the ZnO:Ga/MgO/InGaN heterojunction. The designed n-ZnO:Ga MW/MgO/p-InGaN heterojunction LED can effectively avoid the efficiency droop phenomenon induced by InGaN materials, but bringing about unfavorable disadvantages, such as larger turn-on voltage, lower carrier injection efficiency, lower EL efficiency, and so on. Benefiting from cladding AuNPs, the EL properties of the as-designed LEDs were significantly improved, such as lowering the turn-on voltage, increasing the electronic transport properties and enhancing the EL efficiency. Further, introducing AuNPs can also make the electrical contact between the ZnO:Ga MW and MgO/InGaN layer much more facile and reliable. The resultant EL characteristics of the carefully designed n-AuNPs@ZnO:Ga MW/MgO/p-InGaN heterostructured LEDs that possess merits of having a low-cost, time-saving and simplified preparation process can enable a competitive and promising scheme with prospects of developing high-performance and high-brightness micro- and nanoLEDs.

2 Experimental section

2.1 Sample preparation

The sample of quadrilateral ZnO:Ga wires having high crystalline quality and excellent electrical characteristics was successfully prepared by using a chemical vapor deposition (CVD) method, and the synthesis was accomplished in a standard tubular furnace as we described in previous work.[33,51,52] Highly-purified ZnO, Ga_2O_3 and graphite (C) powders with a weight ratio of 9 : 1 : 10 were used as the uniform source materials. After mixing thoroughly, the source material was contained in a corundum boat. A clean silicon (Si) slice serving as the sample collector was placed on the top surface of the precursor mixture. The boat was laid at the heating area of a quartz tube in the horizontal tube furnace. A carrier gas of high-purity Ar mixed with 5.0% O_2 was flowed into the furnace chamber at a total flow rate of 125 sccm. In the synthesis regime, the tube furnace was heated up to 1100 °C at a ramp rate of 20 °C min^{-1}. The temperature was maintained at 1100 °C for about 1 hour. After the synthesis was finished, the tubular furnace should be cooled slowly to room temperature. ZnO:Ga wires were obtained individually on the Si substrate. The size of the CVD-product ZnO:Ga wires could be controlled by manipulating the preparation conditions, for instance the precursor mixtures, growth time, growth temperature and carrier gas. The length can readily reach up to 2.0 cm, and the cross-sectional sizes change from 0.5 to 50 μm. Besides, the sample of Au nanostructures was chemically synthesized using a seed-mediated method as we previously shown.[53]

2.2 Device fabrication

A new generation green LED light source, which contains a single ZnO:Ga MW and p-type InGaN substrate, was designed. In the device structure, the commercially purchased p-type InGaN chip was employed as a hole

transport supplier.[33,52,54] The p-type InGaN template is a vertically layered structure, which is composed of a sapphire substrate, a p-GaN layer, an AlGaN/InGaN superlattice layer, InGaN quantum wells and an AlGaN layer sequentially.[13,26,55] In the p-InGaN layer, the used AlGaN/InGaN and AlGaN working as electron-blocking layers can be used to appropriately modify the energy band diagram of InGaN-based optoelectronic devices, which is favorable for the injection of holes and the confinement of electrons, respectively. The LED fabrication procedure is as follows. First, a Ni/Au ohmic contact with 40/50 nm in thickness was deposited on the p-type InGaN layer using electron beam heating evaporation. Second, two MgO films with a thickness of about 8 μm were deposited on the InGaN film using electron beam evaporation *via* a shadow mask, and there is a gap distance of ~50 μm between the pre-prepared MgO films. The pre-deposited MgO films were situated along the bilateral sides of the wire. Third, a single ZnO:Ga MW was mechanically laid on the p-InGaN film. Finally, a piece of ITO conductive glass was placed on the top surface of the device inversely. Thus, the deposited MgO films on the bilateral sides of the InGaN layer can work as insulating media to prevent the direct contact between the ITO electrode and InGaN film. In the as-designed LED structure, the Ni/Au film and ITO conductive glass can function as the ohmic contact electrodes for the current injection of the n-ZnO:Ga MW/p-InGaN heterojunction device. A typical device configuration of the designed n-ZnO:Ga MW/p-InGaN heterojunction is depicted in Fig. 1(d).

To engineer the energy-band alignment, an ultrathin MgO layer with a thickness of about 10 nm was inserted into the n-ZnO:Ga/p-InGaN heterojunction by using an electron beam evaporation system. The schematic diagram of the green LED structure based on the as-designed n-ZnO:Ga MW/MgO/p-InGaN heterojunction is shown in Fig. 3(a). Further to optimize the EL properties, an individual ZnO:Ga MW covered with Au nanostructures was used to construct light-emission devices. Accordingly, the schematic illustration of the fabricated n-AuNPs@ZnO:Ga MW/MgO/p-InGaN heterojunction LED is shown in Fig. 5(a).

2.3 Device characterization

Electrical characterization of individual ZnO:Ga wires, the p-InGaN layer and the fabricated LEDs was carried out using a Keysight B1500A sourcemeter system. The optical properties

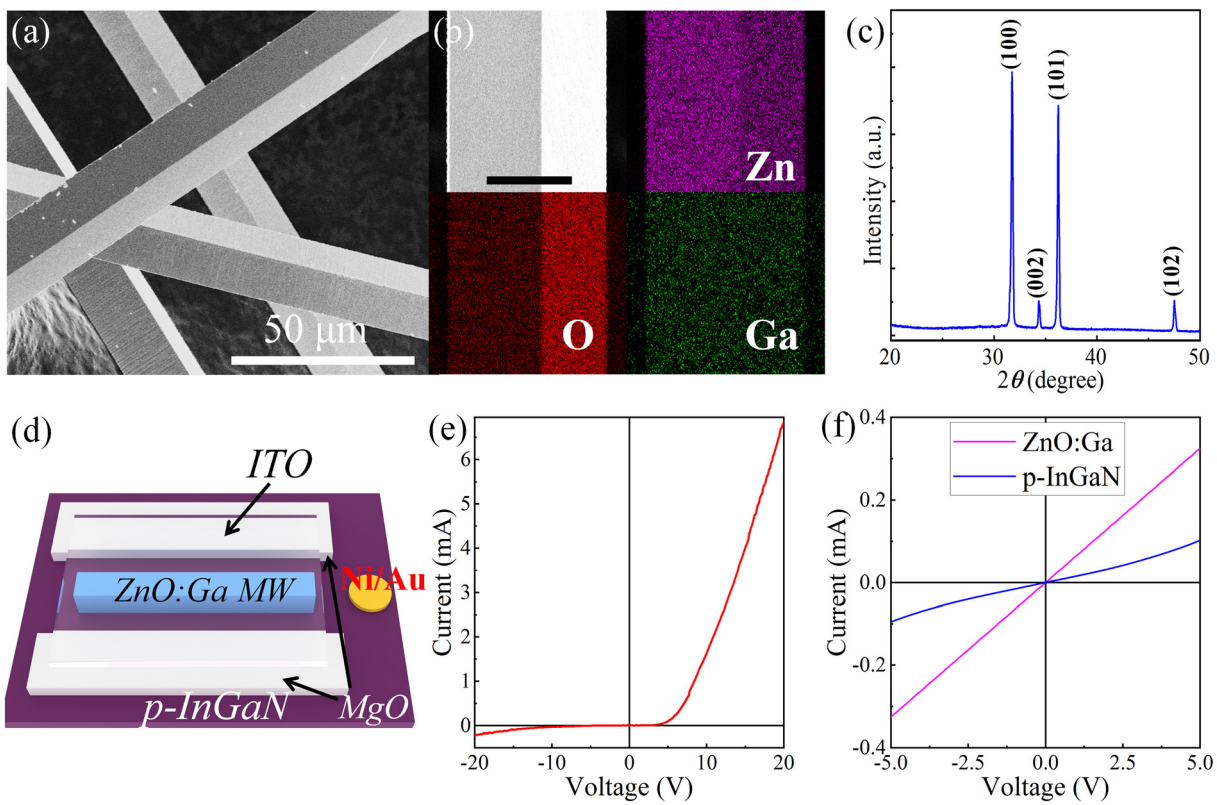

Fig. 1 Sample characterization and LED fabrication. (a) SEM image of individual ZnO:Ga wires showing quadrilateral morphologies. (b) SEM figure and elemental mapping results of a ZnO:Ga wire, which clearly shows uniform composition of Zn, Ga and O elements. (c) XRD result of the as-synthesized ZnO:Ga sample. (d) Schematic view of a kind of green light-emission device, which is composed of a ZnO:Ga wire and a p-InGaN chip. In the device, Ni/Au and ITO served as electrodes for the current injection. (e) The *I*–*V* characteristic curve of the fabricated n-ZnO:Ga MW/p-InGaN heterostructure device, showing diode-like rectifying properties. (f) *I*–*V* characteristic curves of a single ZnO:Ga wire and a p-type InGaN film, respectively.

of the CVD-synthesized ZnO:Ga samples and InGaN layer were measured using a photoluminescence (PL) system, which contains a 325 nm He–Cd laser, a high-resolution LabRAM-UV Jobin-Yvon spectrometer and a high-sensitivity charge-coupled device (CCD). EL characterization of the as-fabricated LEDs was performed using a microspectral detection system, which consists of an ANDOR detector (CCD-13448) and an Omni-λ 500 spectrograph. An optical microscope was employed to capture the EL images of the as-fabricated heterojunction LEDs *via* a CCD camera. In the EL measurement, a direct and continuous current power source was utilized to bias the fabricated emission devices. All the experiments have been carried out at room temperature.

2.4 Theoretical simulation

Finite difference time domain (FDTD) solution was used to simulate the electric field distribution of an isolated and spherical Au nanoparticle, as well as the coupling interaction between an Au nanostructure and a ZnO:Ga wire. The structural models of a spherical Au nanoparticle and an Au nanoparticle placed on a ZnO:Ga wire were also constructed, which were employed to simulate the spatial localization and distribution of electric-field intensities, respectively. In the as-constructed models, the outgoing waves were completely absorbed by the surrounding perfect matched layer (PML). During the simulation, the refractive indexes of ZnO:Ga ($n_{ZnO:Ga}$) and air (n_{air}) were set to 2.35 and 1.0, respectively; the resonance wavelength λ used in the simulation is referred to as the strongest extinction peak, which is shown in Fig. 4(a); the diameter of the Au nanoparticle is measured to be about 50 nm. The complex relative permittivity of the nanostructured Au at the wavelength of λ = 540 nm is $\varepsilon_{Au} = n + ik = 0.55 + 2.38i$ according to the experimentally obtained data.[51,53]

3 Results and discussion

Using a facile CVD method, the sample of ZnO:Ga wires with sharp edges, smooth side facets and a quadrilateral cross-sectional morphology was synthesized individually.[33,51,52] A typical SEM observation of ZnO:Ga wires is shown in Fig. 1(a), showing quadrilateral profiles, sharp edges and smooth side facets. The compositional mapping of a single ZnO:Ga wire was measured using energy-dispersive spectroscopy (EDS). As shown in Fig. 1(b), uniform distribution of Zn, Ga and O elements can be clearly captured.[51] The crystalline phases of the CVD-synthesized ZnO:Ga samples were checked using X-ray diffraction (XRD). The obtained XRD pattern shown in Fig. 1(c) reveals that all diffraction peaks centered at 31.6°, 34.3° and 36.2° can be indexed to wurtzite phase ZnO with good crystallinity. Therefore, individual ZnO:Ga wires with a quadrilateral cross-sectional morphology and good crystallinity have been synthesized.[34,52]

By combining a p-type InGaN film, an individual ZnO:Ga wire was used to construct a kind of green light-emitting device.[33,54] The device structure is schematically depicted in Fig. 1(d). In the device, Ni/Au and ITO served as electrodes for the current injection. The forward bias current–voltage (*I–V*) characteristics of the fabricated n-ZnO:Ga/p-InGaN heterostructural device are presented in Fig. 1(e), exhibiting LED-like rectifying properties. The electronic transport behaviors of a single ZnO:Ga wire and p-InGaN film were studied, respectively. The plotted *I–V* curves shown in Fig. 1(f) reveal typically linear features, thus, an ideal ohmic junction is formed at the ZnO:Ga–In interface (the violet solid line), as well as the ohmic contact feature of the p-InGaN film that is in contact with the Ni/Au electrode. Conclusively, the as-synthesized ZnO:Ga MW can form a p–n heterojunction with the p-type InGaN film (the blue solid line). The turn-on bias voltage of the fabricated n-ZnO:Ga MW/p-InGaN heterojunction is extracted to be about 4.65 V. The rectification ratio is evaluated to be about 50 (the reverse leakage current at −10 V is measured to be about 0.13 mA, while the forward injection current is extracted to be about 6.5 mA). These results exhibit that the rectifying behavior comes from the p–n heterojunction formed between the ZnO:Ga MW and InGaN layer, instead of the metal–semiconductor contact.

When the fabricated n-ZnO:Ga MW/p-InGaN heterojunction LED was forward biased electrically, green light-emission was observed, with the emission regions distributed along the wire body. The emitted photons were collected using a spectrometer by varying the injection current in the scope of 0.2–5.2 mA, and the corresponding EL spectra are presented in Fig. 2(a). The LED emits a typical green light-emission peaking at around ~540 nm, and the spectral full width at half maximum (FWHM) is evaluated to be about 36 nm. The evolution of integrated EL intensity *versus* the operating current is depicted in Fig. 2(b), suggesting that the green light output intensities increase linearly as a function of the injection current. Detailed information on the EL characteristics of the fabricated n-ZnO:Ga MW/p-InGaN LED was studied. Fig. 2(c) shows the variations of the EL peaks and FWHM *versus* the injection current. At an operating current of 0.2 mA, the EL peak wavelength is centered at 544 nm with a FWHM of 36.5 nm. As the injection current reaches up to 5.2 mA, the main EL peaks of the fabricated LED exhibit a visible blue-shift of about 11 nm, which is caused by the reduced polarization-related electric fields in the InGaN layer.[26,56] Meanwhile, the FWHM reveals a slight fluctuation varying from 35.0 to 36.5 nm in terms of different injection currents. The variations observed in the EL emission properties may be caused by the reduced polarization field in the InGaN layer. The combination of ZnO with various kinds of nano- and microstructures and the p-type InGaN substrate could provide an alternative strategy for realizing visible LEDs in the future.

The green EL mechanism of the fabricated n-ZnO:Ga MW/p-InGaN heterojunction LED was researched. First, the optical properties of a single ZnO:Ga wire were tested using a

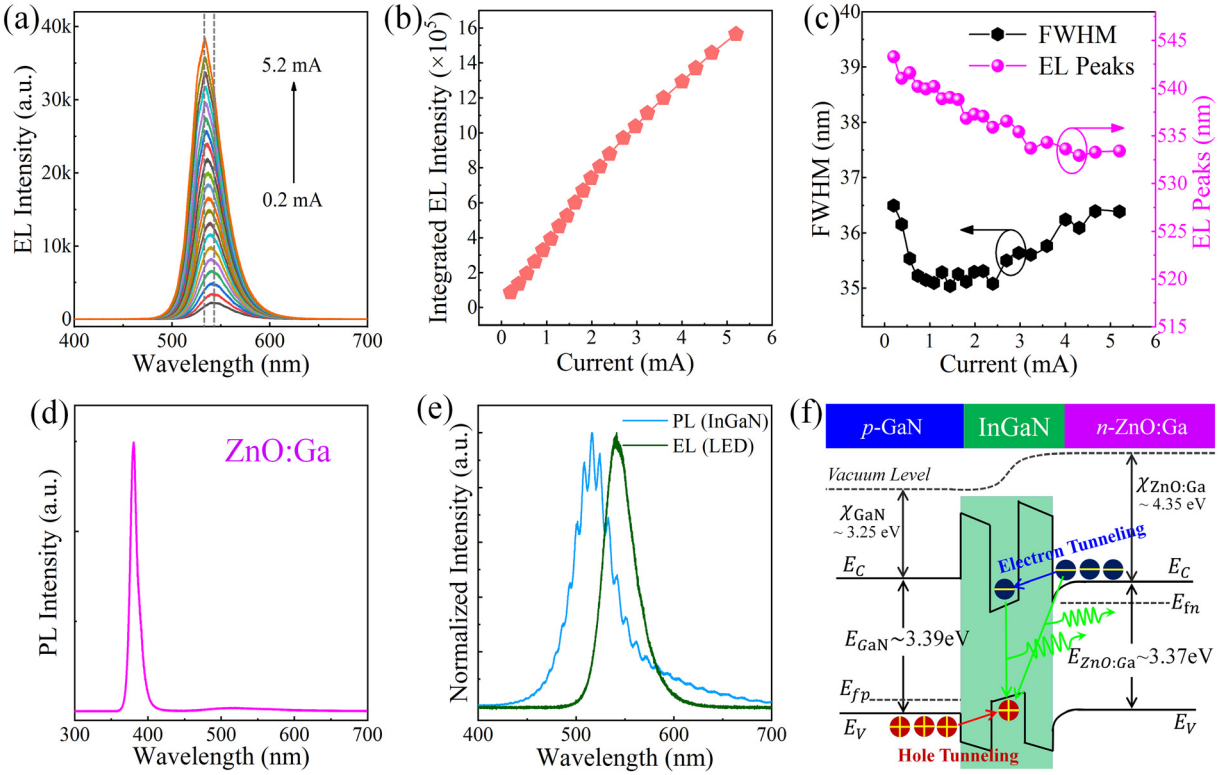

Fig. 2 EL characterization of the fabricated n-ZnO:Ga MW/p-InGaN heterojunction LED. (a) EL spectra of the fabricated LED, the injection current varied from 0.2–5.2 mA. (b) Injection current-dependent integrated EL intensity of the fabricated LED. (c) The variations of EL peaks and the FWHM of the fabricated LED as functions of the operating current. (d) PL result of a single ZnO:Ga wire. (e) Normalized PL intensities of the p-InGaN film and EL of the fabricated LED (the injection current is 4.8 mA) are supplied for comparison. (f) Energy band alignment of the n-ZnO:Ga/p-InGaN heterojunction and carrier injection under a forward bias, respectively.

PL measurement system *via* a 325 nm He–Cd laser. The PL spectrum of a ZnO:Ga wire is shown in Fig. 2(d). It indicates that the dominant PL wavelength peaking at around 378.8 nm can be assigned to the band-edge of ZnO:Ga, and the FWHM is measured to be about 12.0 nm. Meanwhile there is a negligible visible emission. The resulting PL suggests that the CVD-produced ZnO:Ga wires possess excellently good crystalline quality.[34,35] Second, the PL properties of the InGaN layer were further measured. The normalized PL spectrum of p-InGaN and the EL spectrum derived from the as-fabricated n-ZnO:Ga MW/p-InGaN heterojunction LED are given in Fig. 2(e) for comparison. The main PL wavelength of InGaN film peaks at around 516.2 nm under the excitation of a 325 nm He–Cd laser is shown in the figure (the sky-blue solid line). And the green light-emission can be attributed to the as-prepared InGaN quantum well structure. Meanwhile the observed PL spectrum with multimode peaks could be assigned to the much larger refractive index of the InGaN materials.[25,28] The main EL peak is positioned at around 541.0 nm. Thus, a distinct gap of approximately 24.8 nm between the LED EL and InGaN PL wavelengths can be observed. The corresponding line width is measured to be about 32 nm, which is spectrally narrower than that of the EL spectrum of the as-constructed n-ZnO:Ga MW/p-InGaN heterojunction LED. Consequently, the obtained green EL emission cannot be determined either from the ZnO:Ga sample or the InGaN film. The apparent broader EL band achieved in the as-fabricated n-ZnO:Ga MW/p-InGaN LED could be attributed to the combination of the light emission at the side of the InGaN layer and the electron–hole radiative recombination occurring across the band offset at the depletion region of the n-ZnO:Ga/p-InGaN heterointerface.[18,34,54]

To gain a deeper insight into the working principle of green EL and the electronic transport channel of the injected carrier charges, the diagrammatic view of the energy band alignment of the designed n-ZnO:Ga/p-InGaN heterojunction was supplied. The electron affinities ψ of ZnO:Ga and InGaN are $\psi_{ZnO:Ga}$ ~4.35 and ψ_{InGaN} ~3.25 eV, respectively. The energy bandgaps of ZnO:Ga ($E_{ZnO:Ga}$) and InGaN (E_{InGaN}) are ~3.37 and ~2.42 eV, respectively. When n-type ZnO:Ga was in contact with p-type InGaN, a p–n heterojunction could be formed, yielding a band offset toward the heterointerface.[33,50,54] Due to the existence of AlGaN electron blocking layers between ZnO:Ga MW and InGaN quantum well structure, the energy band of the neighbouring ZnO:Ga barrier changes from upward to small downward bending.[18,55] Obviously, a typical staggered type-II heterojunction will be constructed between the ZnO:Ga MW and p-type InGaN film, with the energy band diagram shown in Fig. 2(f). Under a forward bias, the injected electrons are mainly

blocked at the side of the ZnO:Ga MW. However, a slight carrier leakage may occur due to the relatively small conduction band-offset between AlGaN and ZnO:Ga. That is, a few electrons can be tunnelled into the conduction band of the InGaN quantum well layer. Thereby, the presence of electron overflow and/or electron leakage may induce the green light emission occurring at the side of the InGaN layer.[27] In the case of high operating current levels, large quantities of carriers would be input into the n-ZnO:Ga/p-InGaN heterojunction, and the subsequent electron–hole recombination procedure might be accomplished *via* different transition paths: (i) the radiative recombination would be favored to occur across the band offset at the depletion region of n-ZnO:Ga/p-InGaN; (ii) the radiative recombination between the tunnelled electrons and holes may occur in the InGaN quantum well structure.[57,58] Consequently, the observed green light emission in the fabricated LED should originate from the carrier recombination across the band offset at the n-ZnO:Ga/p-InGaN heterointerface and the InGaN layer.

As reported in the previous literature, it has remained extremely challenging to achieve high-brightness, high-efficiency and droop-free green, yellow and red LEDs utilizing conventional InGaN quantum wells due to the relatively larger proportion of In incorporation in InGaN materials and structures.[9,24,27] In particular for the droop effect, the precipitating factors causing the efficiency droop are heavily related to the following possible reasons, containing the quantum confined Stark effect, nonradiative recombination, current crowding effect, serious current leakage, self-heating effect, polarization effect, and limited current injection efficiency.[24,26,55] As mentioned above, the dominating factors for the efficiency droop are presumably the electron leakage and poor hole injection efficiency. In the case of the fabricated n-ZnO:Ga MW/p-InGaN heterojunction LED, the measured electron leakage would cause serious hindrance to the achievement of low-dimensional, high-efficiency and high-brightness green light sources. The origin of the leakage current was studied, which is caused by the electron-tunnelling through the smaller energy barrier of the conduction band off-set at ZnO:Ga/AlGaN.[27,57,58] The larger leakage current at high reverse bias voltage would deteriorate the EL properties. Thus, the much lower EL efficiency may be caused by the competition of carrier radiative recombination occurring in the p-InGaN side and at the n-ZnO:Ga/p-InGaN heterointerface. Besides, the nonuniform electronic contact between the ZnO:Ga MW and InGaN layer in the case of ordinary and direct physical contact may be another possible trigger of the flow of electrons (electron leakage) to the p-type InGaN at a high operating level. Therefore, due to these limitations, the AlGaN film capped on the InGaN quantum well structures may not be the most desirable blocking layer in the as-constructed n-ZnO:Ga MW/p-InGaN heterojunction LEDs.[18,55,59]

MgO is a promising broad-bandgap semiconductor, a good tunneling and spintronics material, which could modulate the heterointerface and retard the electron–hole recombination. The incorporation of ultrathin MgO dielectric layers is already widely used to engineer the current transport/blocking properties in heterostructured optoelectronic devices. Particularly, the use of a MgO buffer layer with a higher conduction band maximum level plays a principal character in electron blocking.[34,54,60] In the present research, the insertion of an additional MgO nanofilm serving as an electron-blocking layer in the n-ZnO:Ga MW/p-InGaN heterojunction can be used to optimize the interfacial characteristics and modulate the EL properties of the fabricated LEDs. The schematic view of the device structure, which is composed of a single ZnO:Ga MW, a MgO buffer layer and a p-InGaN layer, is depicted in Fig. 3(a). The current–voltage characteristics of the device were studied, and the corresponding *I-V* curve is shown in Fig. 3(b). From the figure, a turn-on voltage is measured to be about 8.85 V, which is remarkably larger than that of the n-ZnO:Ga MW/p-InGaN heterojunction (~4.65 V). Regrettably, a relatively lower injection current of ~4.2 mA can be obtained at a forward bias voltage of 20 V. The relatively large turn-on voltage is likely to be due to the insertion of a MgO electron-blocking layer between the ZnO:Ga MW and the p-type InGaN layer. The energy-band diagram of the designed n-ZnO:Ga MW/MgO/p-InGaN heterojunction LED was studied to gain a good understanding of the functional role of inserting a MgO layer, as shown in Fig. 3(c). According to the electron affinities of ZnO:Ga and MgO, the conduction-band offset is derived to be about 3.55 eV.[34,54] Under a forward bias, the injected electrons will be restrained and accumulated at the quasi-Fermi levels (E_{fn}) at the side of the ZnO:Ga MW. The electron-tunneling at the ZnO:Ga/MgO interface is principally forbidden. In the case of the as-constructed n-ZnO MW/MgO/p-GaAs heterojunction, the reverse current would be dramatically suppressed due to the insertion of the MgO layer. Therefore, the light emission occurring at the InGaN side can be ignored.

Under the operation of a forward bias, the EL characterization of the as-fabricated n-ZnO:Ga MW/MgO/p-InGaN LED was measured. Accordingly, Fig. 3(d) shows the EL spectra by varying the injection current in the range of 0.4–7.3 mA. As shown in the EL spectra, a typical green light emission peaking at around 545 nm and a spectral FWHM of about 43 nm can be observed. Further, Fig. 3(e) reveals the variations of EL peaks and FWHM as a function of the injection current. There is no significant shift in the emission peak position with increasing injection current, suggesting a small level of the quantum-confined Stark-effect. The results clearly explain that the fabricated LEDs are much stable. The EL spectra of the fabricated LEDs without and with a MgO buffer layer at an operating current of 4.35 mA are plotted in Fig. 3(f) for comparison. In addition to a clear enhancement of the EL intensity, there is also a slight red shift of the EL wavelength of the LED with a MgO buffer layer. The experimental result indicates that the carrier radiative recombination occurring in the InGaN quantum well structure is effectively suppressed. Thereby, benefiting from the modulation of the MgO layer on the electronic transport properties, the electrons were primarily confined and accumulated in the ZnO:Ga MW. Adding the additional MgO buffer layer, the electron tunneling probability at the n-ZnO:

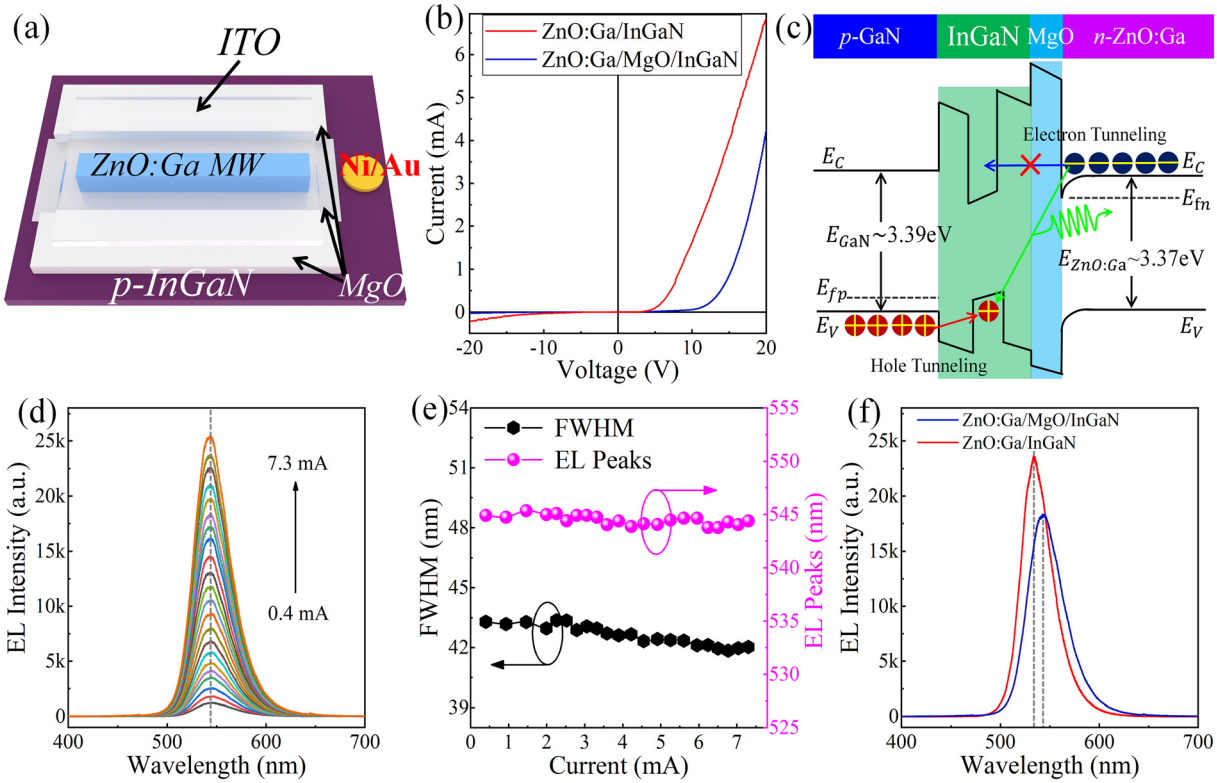

Fig. 3 EL characterization of the fabricated n-ZnO:Ga MW/MgO/p-InGaN heterojunction LED. (a) Schematic illustration of the as-designed p–i–n heterojunction LED, which is based on a single ZnO:Ga wire, MgO buffer layer and p-InGaN film. (b) The plotted *I*–*V* characteristic curves of the fabricated LEDs, in which the device was uninserted and inserted with a MgO nanofilm as a buffer layer. (c) Energy band alignment of the fabricated n-ZnO:Ga/MgO/p-InGaN p–i–n heterojunction. (d) EL spectra of the fabricated n-ZnO:Ga MW/MgO/p-InGaN heterojunction LED with increasing the operating current within the scope of 0.4–7.3 mA. (e) The variations of EL peaks and FWHM of the fabricated LED in terms of the injection current, respectively. (f) EL spectra of the fabricated n-ZnO:Ga MW/p-InGaN and n-ZnO:Ga MW/MgO/p-InGaN heterojunction LEDs are given for comparison. The operating current is 4.35 mA.

Ga/p-InGaN heterointerface could be considered nearly insignificant.[18,54,59]

In the case of inserting a MgO electron blocking layer, the reverse current of the as-constructed n-ZnO:Ga MW/MgO/p-InGaN heterojunction would be dramatically suppressed. However, the turn-on voltage of the fabricated n-ZnO:Ga MW/MgO/p-InGaN heterojunction LED is larger than that of the device structure in the absence of the MgO layer. Meanwhile the electronic transport properties of the device became poorer because of the increased resistance in the presence of the MgO electron blocking layer. Thereby, the introduction of the MgO buffer layer would result in the lower EL efficiency. To improve the LED characteristics of the as-constructed n-ZnO:Ga MW/MgO/p-InGaN heterojunction device, the strategy is to cap nanostructured metals with desired plasmons on the ZnO:Ga MW.[35,51,61] Plasmonic Au nanostructures have attracted ever-increasing attention because of their tunable light harnessing capabilities varying from visible to infrared wavelengths since these are chemically and mechanically stable. In the present research, Au nanoparticles were synthesized chemically using a facile seed-mediated method.[53,62–64] By changing the synthesis conditions, AuNPs with an average diameter of about 50 nm were achieved. The extinction spectrum of AuNPs shown in Fig. 4(a) was measured using an ultraviolet-6300 spectrophotometer. From the extinction spectrum, the main wavelength peak is located at around 538 nm. The corresponding structural morphology of the as-synthesized AuNPs is shown in the inset of Fig. 4(a).

Introducing AuNP decoration, the surface morphology of a single ZnO:Ga MW is further observed in Fig. 4(b). As shown in the figure, AuNPs with uniform distribution can be spin-coated on the wire. The influence of AuNPs on the electrical and optical properties of the ZnO:Ga MW was studied. Fig. 4(c) reveals the *I*–*V* curves of a single ZnO:Ga MW not decorated and decorated with AuNPs. The linear behavior suggests that the contact between the ZnO:Ga MW not covered and covered with AuNPs can form ohmic contact features with In particles serving as electrodes. Because of the relatively higher crystal quality and outstanding electronic transport character of the as-synthesized ZnO:Ga MWs, the localized Schottky barrier formed between Au and ZnO:Ga makes little influence on the current transport properties of a single ZnO:Ga MW. Conclusively, a distinct enhancement of electronic transport properties can be assigned to the surface treatment of capping AuNPs for individual ZnO:Ga MWs.[65–67] The PL properties of a single

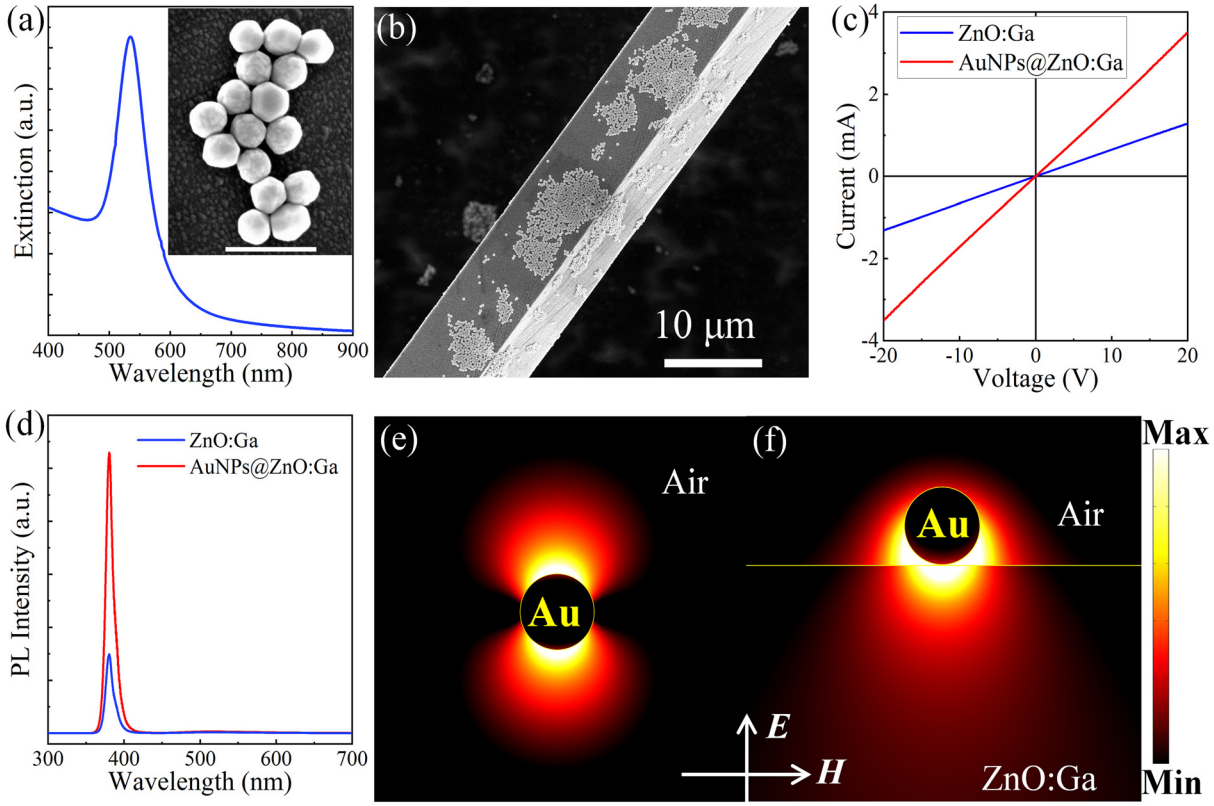

Fig. 4 The influence of AuNPs on the electrical and optical properties of a ZnO:Ga MW. (a) Extinction spectrum of the as-synthesized AuNPs. Inset: SEM image of the AuNPs, and the average diameter of the nanoparticles is evaluated to be about 50 nm. (b) SEM image of a single ZnO:Ga MW covered with AuNPs. (c) *I*–*V* curves of a single ZnO:Ga MW not covered and covered with AuNPs. (d) PL results of a single ZnO:Ga MW not covered and covered with AuNPs. Distribution of the simulated electric-field strength near the surface of a spherical AuNP at an external excitation wavelength of 536 nm (e) without and (f) with the presence of the ZnO:Ga wire.

ZnO:Ga MW not covered and covered with AuNPs were measured using a 325 nm He–Cd laser, and the corresponding PL spectra are depicted in Fig. 4(d). It is indicated that a clear enhancement of the typical near-band emission of the ZnO:Ga MW is obtained. Meanwhile the visible emission is observably suppressed by using AuNP cladding. Thus, the incorporation of AuNPs can act as protective capping and surface passivation of low-dimensional ZnO:Ga materials. The treatment of capping with nanostructured metals is a workable method to enhance the optical properties of a ZnO:Ga MW, including near-band edge emission enhancement and significant suppression of its visible emission. This declares that an obvious number of surface traps were successfully removed. The PL enhancement in a single ZnO:Ga MW covered with AuNPs can be attributed to the cooperative influences of outer surface cleaning modulation, the reduction of non-radiative recombination centers and the increased neutral donor levels.[61,68]

The modulation of AuNP plasmons on the optical and electrical properties of a single ZnO:Ga wire was checked. Numerical simulations of the spatially localized electric-field intensity distribution of an isolated spherical Au nanoparticle, which was spin-coated on a ZnO:Ga wire, were examined using a FDTD solution.[51,61,69] The related parameters are supplied in the Experimental section. Working as the propagating plane wave, the targets of the as-constructed single AuNP and the nanoparticle placed on the ZnO:Ga were illuminated by the incident light. Upon visible light illumination at the plasmonic resonance wavelength of 538 nm, the spatial distribution of near-field electric-field intensity around the AuNP was simulated numerically. When the incident light illuminates on the target (the isolated Au nanosphere), the electric-field E of the incident light along the perpendicular direction can stimulate the conduction band electrons of the Au nanosphere to move toward the surface. When the electrons are accumulated at one side of the particle, the positive charge will be gathered on the other side, yielding a dipole resonance mode plasmonically.[70] As shown in Fig. 4(e), it is obviously illustrated that the calculated electric field is mainly situated at the two sides of the spherical particle due to the simulated optical path along the E-direction. Therefore, the single Au nanoparticle can resonate in a dipole mode.

The study of the plasmon-enhanced near-field concentration of a single AuNP placed on the ZnO:Ga structure was further taken into consideration. The simulated results shown in Fig. 4(f) reveal that the electric field around the AuNP/ZnO:Ga interface is intensely increased. That is, the optical energy is tightly distributed toward the AuNPs/ZnO:Ga

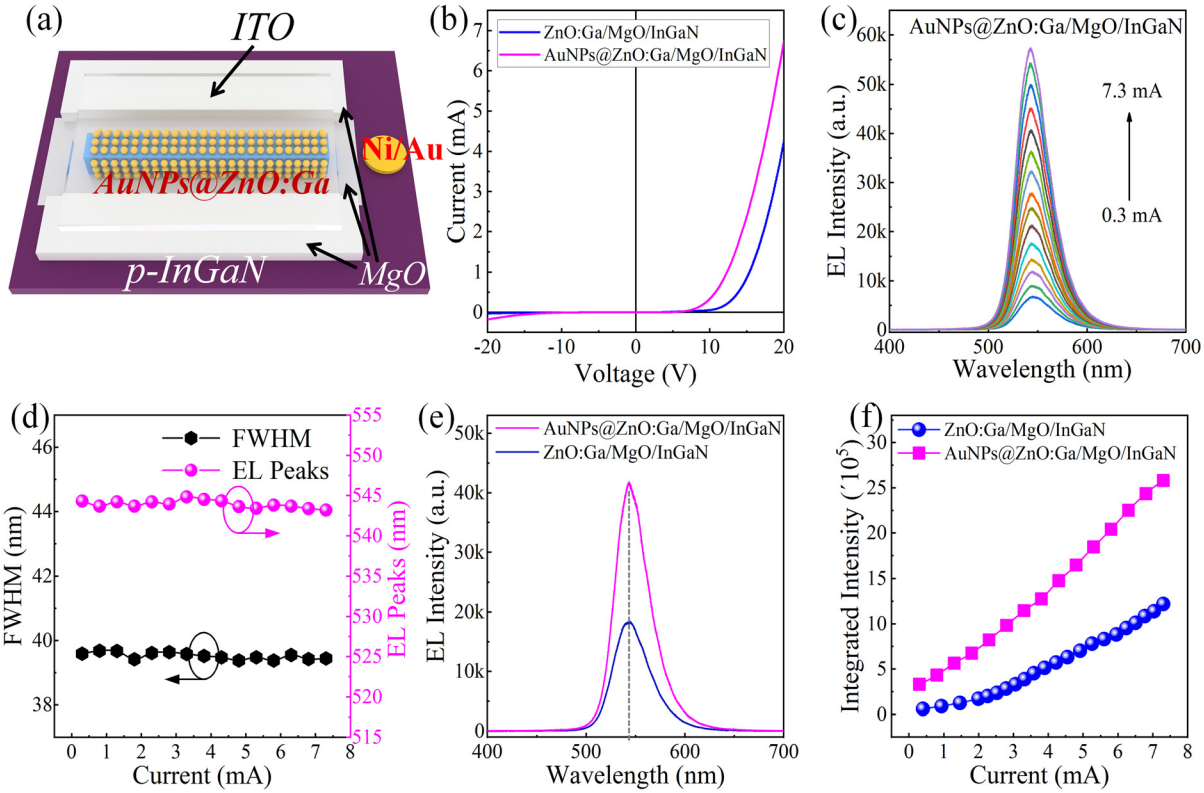

Fig. 5 EL characterization of the fabricated n-AuNPs@ZnO:Ga MW/MgO/p-InGaN heterojunction LED. (a) Schematic illustration of the as-designed n-AuNPs@ZnO:Ga MW/MgO/p-InGaN heterostructured emission device. (b) The plotted *I–V* characteristic curves of the fabricated single ZnO:Ga MW green LEDs, in which the ZnO:Ga MW is not covered and covered with AuNPs. (c) EL spectra of the fabricated n-AuNPs@ZnO:Ga MW/MgO/p-InGaN heterojunction LED with the injection current ranging from 0.3 to 7.3 mA. (d) The variations of EL peaks and FWHM of the LED as a function of the injection current. (e) The EL spectra of the fabricated n-ZnO:Ga MW/MgO/p-InGaN and n-AuNPs@ZnO:Ga MW/MgO/p-InGaN LEDs are given for comparison. The driving current is 4.35 mA. (f) The integrated EL intensities of the fabricated n-ZnO:Ga MW/MgO/p-InGaN and n-AuNPs@ZnO:Ga MW/MgO/p-InGaN LEDs are given for comparison.

interface. And the enhanced near-field intensity can be attributed to the excitation of plasmonic resonance of the deposited AuNPs. For the used Au nanostructures, the plasmonic response wavelengths are principally overlapped with the absorption peaks. The excitation of plasmonic resonance can result in the energy transfer from the absorbed photons plasmonically to the interband excitation of the Au material. The plasmonic behavior of Au nanostructures could cause the excitation of dipole plasmons primarily in terms of nonradiative decay, leading to the loss of plasmonic energy. Thus the efficiency of the photoelectric conversion of Au nanostructures is high, yielding a strong near-field enhancement at visible wavelengths. The contact regions between AuNPs and ZnO:Ga wires exhibit much larger concentration hotspots of the simulated electric-field energies, suggesting that the plasmonic response of metallic nanostructures can mediate optical sensing, strengthening applications in developing high-performance optoelectronic devices.[63,65,70]

The sample of an individual ZnO:Ga MW covered with AuNPs was further utilized to construct a green LED. The schematic diagram of the as-designed LED, which is made of an AuNPs@ZnO:Ga MW, a MgO buffer layer and a p-type InGaN film, is shown in Fig. 5(a). The *I–V* characteristic curves of the fabricated LEDs are presented in Fig. 5(b), in which the used ZnO:Ga MW is not covered and covered with AuNPs. It is clearly shown that the fabricated devices exhibited well-defined rectification properties, yielding a p–i–n heterojunction in the as-fabricated n-ZnO:Ga(AuNPs@ZnO:Ga) MW/MgO/p-InGaN structures. Besides the diode-like rectifying characteristics, the turn-on voltage of the as-fabricated n-AuNPs@ZnO:Ga MW/MgO/p-InGaN LED was estimated to be 6.0 V, which is much smaller than that of the n-ZnO:Ga MW/MgO/p-InGaN heterojunction device (~8.85 eV). At a forward bias voltage of 20 V, the current of the n-AuNPs@ZnO:Ga MW/MgO/p-InGaN LED is measured to be about 6.75 mA, which is much larger than that of the n-ZnO:Ga MW/MgO/p-InGaN LED (~4.28 mA). The electronic transport properties of the fabricated green LEDs are significantly improved by cladding AuNPs on the wires. The combination of the MgO buffer layer and AuNPs can be used to reduce the influence of electron leakage and increase the efficiency of hole injection, which are responsible for the enhanced electrical properties of the fabricated emission devices.

The emitted photons of the fabricated n-AuNPs@ZnO:Ga MW/MgO/p-InGaN heterojunction LED were recorded with

the operating current in the range of 0.3–7.3 mA. The EL spectra shown in Fig. 5(c) exhibit a strong green light emission peaking at 545 nm. Detailed characteristics of the EL emissions are further shown in Fig. 5(d). From the figure, little variation of the EL wavelengths *vs.* injection current could be observed. Similarly, the corresponding FWHM changes hardly at all. Fig. 5(e) shows the EL spectra of the AuNP-enhanced LEDs at a fixed injection current of 4.35 mA. As shown in the figure, the EL intensity of the LED with AuNP cladding is much higher than that of the LED without AuNP decoration. The AuNP-enhanced EL characteristics of the fabricated n-AuNPs@ZnO:Ga MW/MgO/p-InGaN heterojunction LED can be confirmed using the integrated EL intensity, as shown in Fig. 5(f). The larger increase in EL intensity can be attributed to the coupling between the emitted photons and the AuNP plasmons because of the charge density oscillations of the spatially localized plasmonic modes, which have been excited in the AuNPs.[63,64] Therefore, the introduction of AuNPs showing a visible plasmonic response can be utilized to increase the EL properties of the fabricated n-AuNPs@ZnO:Ga MW/MgO/p-InGaN heterojunction LED.

When biased electrically, the optical images of the resulting LEDs were captured using a CCD digital camera *via* an optical microscope objective. Fig. 6(a) shows the optical microscopy figures of the fabricated n-ZnO:Ga MW/MgO/p-InGaN LED by varying the injection current within the scope of 0.4–5.0 mA. With the help of a high-definition CCD camera, evidently bright and green light emission from the wire body can be obtained. The light-emission regions are distributed along the wire, and their intensity is increased. Regrettably, a few dark regions along the wires, which were observed in the microscopy EL images, resulted from the nonuniform electronic contact at the interface. By incorporating AuNPs on the ZnO:Ga wire, significantly increased lighting brightness and emission regions of the n-AuNPs@ZnO:Ga MW/MgO/p-InGaN LED can be achieved, and the corresponding optical microscopy photographs are collected and shown in Fig. 6(b), in which the injection current varied from 0.2 to 2.8 mA. Bright and green lighting can be certainly seen from the as-fabricated n-AuNPs@ZnO:Ga MW/MgO/p-InGaN LED. The bright green emission is observed clearly across the entire wire body and its luminescence intensity increased by increasing the injection current. It needs to be emphasized that the dark regions captured in the n-AuNPs@ZnO:Ga MW/MgO/p-InGaN LED were greatly reduced. It is envisioned that the incorporation of the MgO electron blocking layer and AuNP cladding with optimized design can be exploited to effectively engineer the barrier height of a heterogeneous semiconductor interface in the case of n-ZnO:Ga/p-InGaN heterostructured emission devices, and can result in high-brightness LEDs with significantly increased performances. The combination of the individual ZnO:Ga wire and p-InGaN substrate can enable

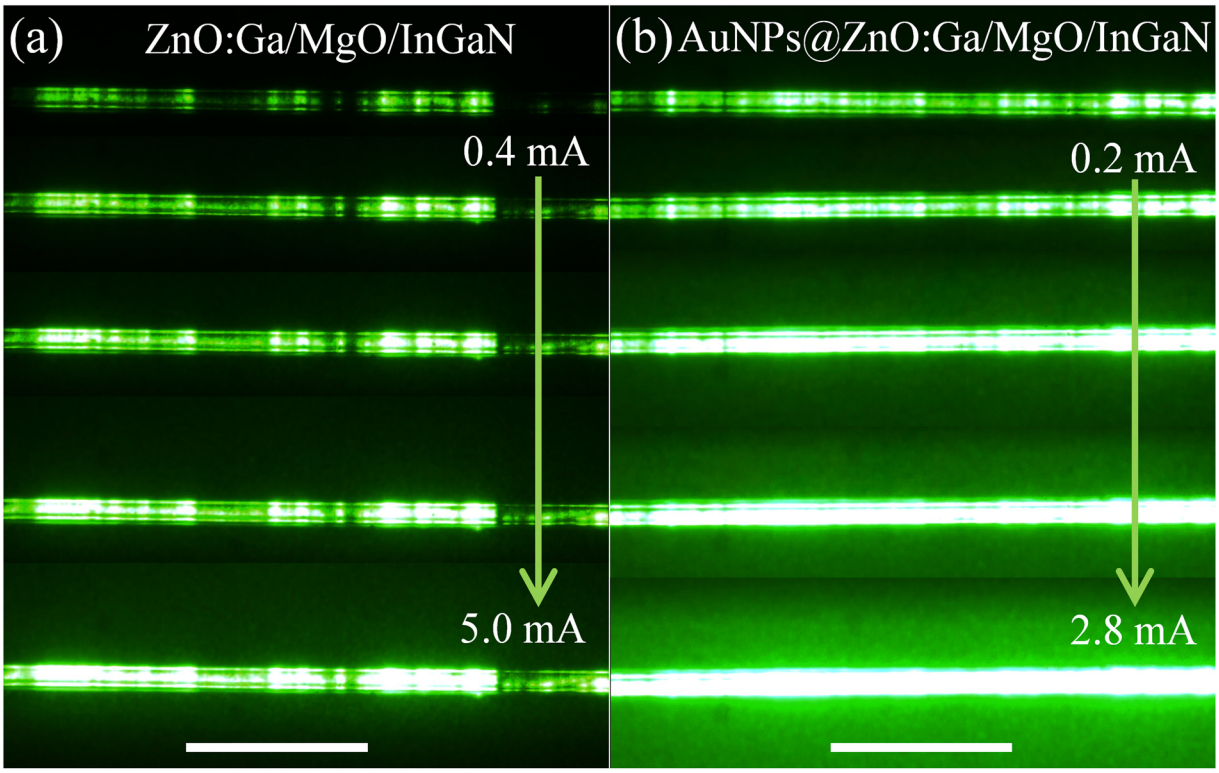

Fig. 6 (a) Optical photographs of the fabricated n-ZnO:Ga MW/MgO/p-InGaN LED with increasing the forward-biased current in the range of 0.4–5.0 mA. (b) Optical photographs of the fabricated n-AuNPs@ZnO:Ga MW/MgO/p-InGaN LED with increasing the forward-biased current in the range of 0.2–2.8 mA. The scale bar is 100 μm.

brand-new possibilities and opportunities for developing nano- and microLEDs operating at visible wavelengths while benefiting from the scalability of mature manufacturing p-type GaN and InGaN/GaN preparation technology.

4 Conclusions

In conclusion, we have proposed and investigated high-efficiency, stable and droop-free green light sources, which are constructed on account of the n-AuNPs@ZnO:Ga MW/MgO/p-InGaN heterojunction. The results exhibited that the proposed LED structure has markedly enhanced EL properties by comparing it with a commonly used n-ZnO:Ga MW/p-InGaN heterojunction. The insertion of MgO buffer layer is thought to be an effective barrier height for the confinement and accumulation of the injected electrons in the ZnO:Ga wire and increasing the holes tunneling into the InGaN layer from the p-type region in the proposed LED structure. The additional insertion of a MgO buffer layer can effectively prevent the carrier loss over heterostructure barriers at the n-ZnO:Ga/p-InGaN interface, which is treated as a compensation for the AlGaN electron blocking layer; while cladding AuNPs can optimize device performances, such as lowering the turn-on voltage, increasing current injection and passivating interfacial defects. Particularly, the AuNPs serving as a plasmonically active component can effectively magnify the LED green light-emission, thus increasing the EL efficiency. The combination of the MgO buffer layer and metallic nanostructure cladding in the as-designed LEDs is used to tailor the energy-band alignment, enhance the electronic characteristics, modulate the carrier recombination path and strengthen the EL emissions in a carefully designed n-ZnO:Ga MW/p-InGaN heterostructure. The presented research provides an alternative scheme to design high-performance visible light sources based on ZnO micro/nanostructures benefiting from interfacial engineering and nanostructured metal cladding.

Author contributions

Xingjie Liu: conceptualization, methodology, sample preparation, structural and device characterization, formal analysis, writing – original draft preparation. Maosheng Liu: methodology, formal analysis, data curation, conceptualization. Rongde Zhu: sample preparation, structural and device characterization. Binghui Li: conceptualization, supervision, resources, editing. Peng Wan: sample preparation, structural and device characterization. Daning Shi: supervision, funding acquisition, editing. Caixia Kan: conceptualization, funding acquisition, editing, supervision. Mingming Jiang: conceptualization, supervision, resources, methodology, data curation, funding acquisition, writing – review & editing, supervision.

Conflicts of interest

There are no conflicts to declare.

Acknowledgements

This study was supported by the National Natural Science Foundation of China (Grant Nos. 11974182 and 11874220), the Fundamental Research Funds for the Central Universities (No. NC2022008), and the Funding for Outstanding Doctoral Dissertation in NUAA (BCXJ22-14).

References

1 W. Yao, L. Wang, Y. Meng, S. Yang, X. Liu, H. Niu and Z. Wang, *CrystEngComm*, 2021, **23**, 2360–2366.
2 J. Li, N. Gao, D. Cai, W. Lin, K. Huang, S. Li and J. Kang, *Light: Sci. Appl.*, 2021, **10**, 129.
3 M. Wurtele, T. Kolbe, M. Lipsz, A. Kulberg, M. Weyers, M. Kneissl and M. Jekel, *Water Res.*, 2011, **45**, 1481–1489.
4 Z. Wu, S. Lu, P. Yang, P. Tian, L. Hu, R. Liu, J. Kang and Z. Fang, *CrystEngComm*, 2019, **21**, 244–250.
5 P. Li, A. David, H. Li, H. Zhang, C. Lynsky, Y. Yang, M. Iza, J. S. Speck, S. Nakamura and S. P. DenBaars, *Appl. Phys. Lett.*, 2021, **119**, 231101.
6 H. Chang, Z. Liu, S. Yang, Y. Gao, J. Shan, B. Liu, J. Sun, Z. Chen, J. Yan, Z. Liu, J. Wang, P. Gao, J. Li, Z. Liu and T. Wei, *Light: Sci. Appl.*, 2022, **11**, 88.
7 E. Barrigon, M. Heurlin, Z. Bi, B. Monemar and L. Samuelson, *Chem. Rev.*, 2019, **119**, 9170–9220.
8 K. H. Li, X. Liu, Q. Wang, S. Zhao and Z. Mi, *Nat. Nanotechnol.*, 2015, **10**, 140–144.
9 A. Pandey, Y. Malhotra, P. Wang, K. Sun, X. Liu and Z. Mi, *Photonics Res.*, 2022, **10**, 1107–1116.
10 I. M. Hoiaas, A. Liudi Mulyo, P. E. Vullum, D.-C. Kim, L. Ahtapodov, B.-O. Fimland, K. Kishino and H. Weman, *Nano Lett.*, 2019, **19**, 1649–1658.
11 J. Wang, M. Wang, F. Xu, B. Liu, J. Lang, N. Zhang, X. Kang, Z. Qin, X. Yang, X. Wang, W. Ge and B. Shen, *Light: Sci. Appl.*, 2022, **11**, 71.
12 D. Almalawi, S. Lopatin, S. Mitra, T. Flemban, A.-M. Siladie, B. Gayral, B. Daudin and I. S. Roqan, *ACS Appl. Mater. Interfaces*, 2020, **12**, 34058–34064.
13 Y. Sun, K. Zhou, M. Feng, Z. Li, Y. Zhou, Q. Sun, J. Liu, L. Zhang, D. Li, X. Sun, D. Li, S. Zhang, M. Ikeda and H. Yang, *Light: Sci. Appl.*, 2018, **7**, 13.
14 S. Lu, X. Jiang, Y. Wang, K. Huang, N. Gao, D. Cai, Y. Zhou, C. C. Yang, J. Kang and R. Zhang, *Nanoscale*, 2022, **14**, 653–662.
15 G. Zhu, J. Li, J. Li, J. Guo, J. Dai, C. Xu and Y. Wang, *Opt. Lett.*, 2018, **43**, 647–650.
16 S. Zhang, Y. Li, P. Hu, Z. Tian, Q. Li, A. Li, Y. Zhang and F. Yun, *Photonics Res.*, 2021, **9**, 432–438.
17 Q. Cai, H. You, H. Guo, J. Wang, B. Liu, Z. Xie, D. Chen, H. Lu, Y. Zheng and R. Zhang, *Light: Sci. Appl.*, 2021, **10**, 94.
18 J. Wang, M. Feng, R. Zhou, Q. Sun, J. Liu, Y. Huang, Y. Zhou, H. Gao, X. Zheng, M. Ikeda and H. Yang, *Photonics Res.*, 2019, **7**, B32–B35.

19 J. Stachurski, S. Tamariz, G. Callsen, R. Butte and N. Grandjean, *Light: Sci. Appl.*, 2022, **11**, 114.
20 C. Zhao, T. K. Ng, N. Wei, A. Prabaswara, M. S. Alias, B. Janjua, C. Shen and B. S. Ooi, *Nano Lett.*, 2016, **16**, 1056–1063.
21 X. Liu, Y. Sun, Y. Malhotra, A. Pandey, P. Wang, Y. Wu, K. Sun and Z. Mi, *Photonics Res.*, 2022, **10**, 587–593.
22 H. Son, P. Uthirakumar, A. Polyakov, J. H. Park, K. H. Lee and I.-H. Lee, *Appl. Surf. Sci.*, 2022, **592**, 153248.
23 F. F. Qin, G. Y. Zhu, J. B. Yang, L. Wei, Q. N. Cui and Y. J. Wang, *Nanoscale*, 2022, **14**, 1921–1928.
24 A. Polyakov, L. Alexanyan, M. Skorikov, A. Chernykh, I. Shchemerov, V. Murashev, T.-H. Kim, I.-H. Lee and S. Pearton, *J. Alloys Compd.*, 2021, **868**, 159211.
25 M. Sheen, Y. Ko, D.-U. Kim, J. Kim, J.-H. Byun, Y. Choi, J. Ha, K. Y. Yeon, D. Kim, J. Jung, J. Choi, R. Kim, J. Yoo, I. Kim, C. Joo, N. Hong, J. Lee, S. H. Jeon, S. H. Oh, J. Lee, N. Ahn and C. Lee, *Nature*, 2022, **608**, 56–61.
26 T. Aggarwal, A. Udai, P. K. Saha, S. Ganguly, P. Bhattacharya and D. Saha, *ACS Appl. Mater. Interfaces*, 2022, **14**, 13812–13819.
27 X. Liu, Y. Sun, Y. Malhotra, A. Pandey, Y. Wu, K. Sun and Z. Mi, *Appl. Phys. Lett.*, 2021, **119**, 141110.
28 Y.-H. Ra, R. T. Rashid, X. Liu, S. M. Sadaf, K. Mashooq and Z. Mi, *Sci. Adv.*, 2020, **6**, eaav7523.
29 Z. Li, X. Zhang, Y. Kang, C. C. Yu, Y. Wen, M. Hu, D. Meng, W. Song and Y. Yang, *Adv. Sci.*, 2021, **8**, 2002631.
30 D. Wu, J. Guo, C. Wang, X. Ren, Y. Chen, P. Lin, L. Zeng, Z. Shi, X. J. Li, C.-X. Shan and J. Jie, *ACS Nano*, 2021, **15**, 10119–10129.
31 C. Ji, C. Liang, Q. Song, H. Gong, N. Liu, F. You, D. Li and Z. He, *Sol. RRL*, 2021, **5**, 2100072.
32 Y. J. Hwang, C. H. Wu, C. Hahn, H. E. Jeong and P. Yang, *Nano Lett.*, 2012, **12**, 1678–1682.
33 M. Liu, M. Jiang, Y. Liu, K. Tang, D. N. Shi and C. Kan, *ACS Appl. Nano Mater.*, 2021, **4**, 11168–11179.
34 X. Zhou, M. Jiang, J. Wu, M. Liu, C. Kan and D. Shi, *Opt. Express*, 2022, **30**, 18273–18286.
35 X. Zhou, M. Jiang, K. Xu, M. Liu, S. Sha, S. Cao, C. Kan and D. N. Shi, *Light: Sci. Appl.*, 2022, **11**, 198.
36 B. Nikoobakht, R. P. Hansen, Y. Zong, A. Agrawal, M. Shur and J. Tersoff, *Sci. Adv.*, 2020, **6**, eaba4346.
37 Y. Chen, L. Su, M. Jiang and X. Fang, *J. Mater. Sci. Technol.*, 2022, **105**, 259–265.
38 S. Nadupalli, S. Repp, S. Weber and E. Erdem, *Nanoscale*, 2021, **13**, 9160–9171.
39 Z. Zhang, Y. Ning and X. Fang, *J. Mater. Chem. C*, 2019, **7**, 223–229.
40 M. C. Newton and P. A. Warburton, *Mater. Today*, 2007, **10**, 50–54.
41 C. Xu, J. Dai, G. Zhu, G. Zhu, Y. Lin, J. Li and Z. Shi, *Laser Photonics Rev.*, 2014, **8**, 469–494.
42 B. Zhao, F. Wang, H. Chen, L. Zheng, L. Su, D. Zhao and X. Fang, *Adv. Funct. Mater.*, 2017, **27**, 1700264.
43 D. Vanmaekelbergh and L. K. van Vugt, *Nanoscale*, 2011, **3**, 2783–2800.
44 M. Ma, J. Tu, Y. Yuan, X. Wang, K. Li, F. Mao and Z. Zeng, *J. Power Sources*, 2008, **179**, 395–400.
45 W. Ouyang, J. Chen, Z. Shi and X. Fang, *Appl. Phys. Rev.*, 2021, **8**, 031315.
46 M. R. Alenezi, A. S. Alshammari, T. H. Alzanki, P. Jarowski, S. J. Henley and S. R. P. Silva, *Langmuir*, 2014, **30**, 3913–3921.
47 J.-B. Yu, M. Sun, M. Yu, M. Yang, H. Yu, Y. Yang, X.-T. Dong and L. Xia, *J. Alloys Compd.*, 2022, **920**, 165884.
48 Z. Yao, M. Xia, Z. Xiong, Y. Wu, P. Cheng, Q. Cheng, J. Xu, D. Wang and K. Liu, *ACS Omega*, 2022, **7**, 3030–3036.
49 S. Rajaambal, M. Mapa and C. S. Gopinath, *Dalton Trans.*, 2014, **43**, 12546–12554.
50 J. Kang, V. Dang, H. Li, S. Moon, P. Li, Y. Kim, C. Kim, H. Choi, Z. Liu and H. Lee, *Nano Convergence*, 2016, **3**, 34.
51 Z. Sun, M. Jiang, W. Mao, C. Kan, C. Shan and D. Shen, *Photonics Res.*, 2020, **8**, 91–102.
52 K. Tang, P. Wan, C. Kan, M. Liu, D. Shi and M. Jiang, *Appl. Phys. Lett.*, 2022, **120**, 011105.
53 Y. Ni, C. Kan, L. He, X. Zhu, M. Jiang and D. Shi, *Photonics Res.*, 2019, **7**, 558–565.
54 J. Li, B. Li, M. Meng, L. Sun and M. Jiang, *Opt. Express*, 2022, **30**, 24773–24787.
55 J.-Y. Chang, Y.-A. Chang, T.-H. Wang, F.-M. Chen, B.-T. Liou and Y.-K. Kuo, *Opt. Lett.*, 2014, **39**, 497–500.
56 I. Manglano Clavero, C. Margenfeld, J. Quatuor, H. Spende, L. Peters, U. T. Schwarz and A. Waag, *ACS Appl. Mater. Interfaces*, 2022, **14**, 9272–9280.
57 A. Pandey, W. J. Shin, J. Gim, R. Hovden and Z. Mi, *Photonics Res.*, 2020, **8**, 331–337.
58 Y. Zhang, S. Krishnamoorthy, F. Akyol, J. M. Johnson, A. A. Allerman, M. W. Moseley, A. M. Armstrong, J. Hwang and S. Rajan, *Appl. Phys. Lett.*, 2017, **111**, 051104.
59 L. He, K. Zhang, H. Wu, C. He, W. Zhao, Q. Wang, S. Li and Z. Chen, *J. Mater. Chem. C*, 2021, **9**, 7893–7899.
60 S. Huang, B. Kang, L. Duan and D. Zhang, *J. Colloid Interface Sci.*, 2021, **583**, 178–187.
61 C. X. Xu, F. F. Qin, Q. X. Zhu, J. F. Lu, Y. Y. Wang, J. T. Li, Y. Lin, Q. N. Cui, Z. L. Shi and A. G. Manohari, *Nano Res.*, 2018, **11**, 3050–3064.
62 N. Yang, C. Deeb, J.-L. Pelouard, N. Felidj and M.-P. Pileni, *ACS Nano*, 2017, **11**, 7797–7806.
63 Z. Shi, Y. Li, S. Li, X. Li, D. Wu, T. Xu, Y. Tian, Y. Chen, Y. Zhang, B. Zhang, C. Shan and G. Du, *Adv. Funct. Mater.*, 2018, 1707031.
64 A. H. Park, S. Baek, G. B. Choi, Y. A. Kim, J. Lim and T. H. Seo, *Appl. Phys. Lett.*, 2021, **119**, 181104.
65 A. Pescaglini, A. Martin, D. Cammi, G. Juska, C. Ronning, E. Pelucchi and D. Iacopino, *Nano Lett.*, 2014, **14**, 6202–6209.
66 S.-H. Lee, S. W. Lee, T. Oh, S. H. Petrosko, C. A. Mirkin and J.-W. Jang, *Nano Lett.*, 2018, **18**, 109–116.
67 L. J. Brillson and Y. Lu, *J. Appl. Phys.*, 2011, **109**, 121301.
68 A. P. Abiyasa, S. F. Yu, S. P. Lau, E. S. P. Leong and H. Y. Yang, *Appl. Phys. Lett.*, 2007, **90**, 231106.
69 X. Zhou, M. Jiang, Y. Wu, K. Ma, Y. Liu, P. Wan, C. Kan and D. Shi, *Nanoscale Adv.*, 2020, **2**, 1340–1351.
70 H. T. B. Do, D. Wen Jun, Z. Mahfoud, W. Lin and M. Bosman, *Nanoscale*, 2021, **13**, 2801–2810.